
Article:
Nair, S.S., Patel, V.I. and Wang, J. (2016) Post-Demagnetization Performance Assessment for Interior Permanent Magnet AC Machines. IEEE Transactions on Magnetics, 52 (4). 8102810. ISSN: 0018-9464

https://doi.org/10.1109/TMAG.2015.2505245

Post Demagnetization Performance Assessment for Interior Permanent Magnet AC Machines

Sreeju S. Nair, *Student Member*, *IEEE*, Vipulkumar I. Patel, *Member, IEEE*, Jiabin Wang, *Senior Member, IEEE*

Department of Electronic and Electrical Engineering, The University of Sheffield, Sheffield, S1 3JD, United Kingdom

This paper assesses post demagnetization performance of Interior Permanent Magnet (IPM) AC machines by employing the more accurate recoil line approach based on 2-D transient finite element (FE) analysis. The method predicts continuous demagnetization of each magnet element undergoing partial demagnetization and evaluates the machine behavior after an event of short-circuit faults across its terminals. Along with the short-circuit faults, a failure in drive controller or position sensor which may lead to a reverse voltage across the machine terminals that can eventually be more fatal and can cause significant reduction in the performance due to high levels of demagnetization, is analyzed as the worst case scenario. The FE predicted post demagnetization performance is validated by experimental measurements in which a 6- phase Interior Permanent Magnet machine designed for EV traction is allowed to lose its synchronization with the inverter when forced to operate on a torque–speed envelope which is way beyond the drive voltage setting.

Index Terms— **Field Weakening, Finite Element Analysis, Interior Permanent Magnet, Inverter failure, Partial demagnetization, Short-Circuit Faults.**

I. Introduction

Interior Permanent magnet (IPM) brushless machines have increasingly been used in transportation applications such as electric and hybrid vehicle traction [1-3], ship propulsion [4], and also aerospace actuation [5]. These machines can be operated in a wide range of speed especially in constant power region [6] compared to the surface mounted permanent magnet (SPM) machines by employing field weakening control [7],[8]. However the machine temperature can increase during continuous operations at higher speeds since the machine iron loss increases with speed and only a part of the armature current is being utilized for producing the useful torque while the rest is required for controlling the main flux to limit the voltage, which results in more copper loss.

A number of recent IPM brushless machines for traction employs fractional slot concentrated winding configurations [9-11], which produces a large number of lower and higher order space harmonics in the stator magneto-motive-force (MMF). These harmonics can deeply penetrate in to the rotor magnets and produce significant eddy current losses [12-14] which may, in turn, lead to increased temperatures especially at higher speeds. The increase in temperature can shift the operating point of each magnet segment of the machine to a lower BH curve with an increased knee point flux density value corresponding to its operating temperature.

The introduction of *d*-axis current to control the air-gap flux at deep field weakening operation may push the magnet flux density towards the vicinity of the knee point. Hence IPM machines are designed with adequate demagnetization withstand capability at its maximum operating temperature and at its maximum speed when filed weakening control is employed [8], [9], [15] and [16].

The risk of irreversible demagnetization can be further intensified in the event of a transient short circuit in field weakening operations [17]. Under the event of a sudden short circuit due to the inverter failure while operating at its peak torque, the transient currents in machine phases can be much higher than its maximum rating and the resultant large *d*-axis current may cause partial demagnetization [18]. The extent of demagnetization is dependent on the magnet operating temperature under such conditions. A more serious event may occur if the inverter loses its synchronization with the machine back EMF, resulting into an opposite voltage being applied at the terminals and developing a sudden surge of currents in the phases. Hence a comprehensive assessment of partial demagnetization at the worst operating condition is necessary at the design stage to understand and to minimize its impact.

There exist a number of demagnetization models in the literature for assessing the risk of partial irreversible demagnetization in permanent magnet (PM) machines. The models described in [19] and [20] aimed to diagnose partial demagnetization in a PM machine based on the torque spectra and the magnetic circuit characteristics, respectively, under an event leading to partial demagnetization. While the consequence of the partial demagnetization can be quantified by these approaches, the demagnetization patterns and their causes are not analyzed. An analytical approach to assess the partial demagnetization by superposing the armature reaction fields in the magnets for a quasi-Halbach magnetized tubular PM machine described in [21]. The analytical approach is not applicable to IPM machines with complex rotor geometry and high level of magnetic saturation. Demagnetization assessment for various IPM rotor types is carried out using average flux density distribution in different magnet segments at various load angles in [22]. However, the approach does not consider the direction of flux density with respect to the direction of magnetization, hence leading to inaccurate results for partial irreversible demagnetization. All these models predict partial demagnetization when the magnet operating point along the B-H curve goes below the knee point flux density. However they are not capable of predicting the extent of partial demagnetization because the magnets are not completely demagnetized even if they operate below their knee points. Consequently, they cannot be used to predict the post demagnetization performance of a PM machine.

Manuscript received August 19, 2015. Corresponding author: S. S. Nair
e- mail: ssnair1@sheffield.ac.uk,
Digital Object Identifier inserted by IEEE

To address this problem, a number of demagnetization models have been proposed in literature to track the history of partial demagnetization, hence, providing a means for predicting post demagnetization performance. S. Ruoho *et al.* [23] compares a number of simplified demagnetization models for an overloaded and overheated SPM machine. The most promising model among them capable of tracking history-dependent hysteresis considers both the magnitude and direction of magnetization of permanent magnet but it fails to describe the Nd–Fe–B magnet behaviour accurately. A model reported by K. Gyu-Hong *et al.* in [24] accounts for the change in remanent flux density of the magnet elements when they operate below the Knee point. Y. Zhilichev in [25] employed recoil lines to predict the magnetization vector when the operating points have fallen below the knee of the demagnetization B-H curve. This method is incorporated in [26] and [27] to evaluate the combined effect of temperature and the demagnetization in PM machines. However, no experimental results on the post-demagnetization performance are provided for the validation of these models.

Demagnetization assessment of an IPM machine under stator turn fault conditions is performed in [28] and [29], and owing to a controller limited fault current is evaluated in [30] by updating the remanence of the magnet elements following partial demagnetization. The post-fault performance is assessed and verified by experiments with limited accuracy. A similar concept is used to assess demagnetization under different fault conditions in [31] and [32] for a distributed wound IPM machine, but no experimental validation of post-fault performance is given.

Demagnetization assessment of PM brushless machines employing fractional-slot winding configuration under worst case faults, and its comparison with distributed wound PM machines is reported in [18] . However, this method is not qualified to evaluate a continuous demagnetization procedure as the remanence of each permanent magnet element is not updated in the event of partial demagnetization and the new value is not incorporated in the subsequent step of the analysis. This can result in the overestimation of the extent of demagnetization as the short circuit current in an event of fault is not being reduced after each subsequent step when the partial demagnetization occurs.

To date the worst case demagnetization scenario for IPMs has not been comprehensively assessed. In addition, the post demagnetization performance evaluated in the literature is mostly confined to the study of change in back EMFs and the reduction in torque as a result of partial demagnetization has not been quantified extensively.

The objectives of this paper are to comprehensively assess the risk of partial irreversible demagnetization for the IPM brushless machines under an event of symmetrical faults by employing a continuous demagnetization model and to predict the post fault performance. The results obtained are compared with the method described in [18]. The performance of the machine after a drive failure, resulting in the loss of synchronization of the applied voltage with the machine, is evaluated as the worst case failure. The results from the FE model are validated by experiments in which the machine is forced to lose its synchronization when operating at high speed with excessive current in the deep field weakening. Finally the de-rating of the machine after partial demagnetization is quantified for its post-fault operation.

II. Continuous Demagnetization Analyses Using 2-D FEA

In order to assess the continuous demagnetization it is necessary to track the flux density in the direction of magnetization for every element of the magnets in the FE model of a machine distinctly with respect to the knee point flux density at a specified operating temperature. In the presence of armature reaction field, if the flux density of any magnet element evaluated has gone below the knee point flux density as shown in the Fig.1, it will be operated on a new BH curve with reduced remanent flux density. The new BH curve, denoted as the dotted line in Fig. 1, is determined by the recoil line [33] and its intersection with the vertical axis. This necessitates the model to keep the history of partial demagnetization for every element of the magnets and to reassign its magnetization levels in an efficient way to assess the demagnetization levels and to compute the machine performance under extreme or fault conditions.

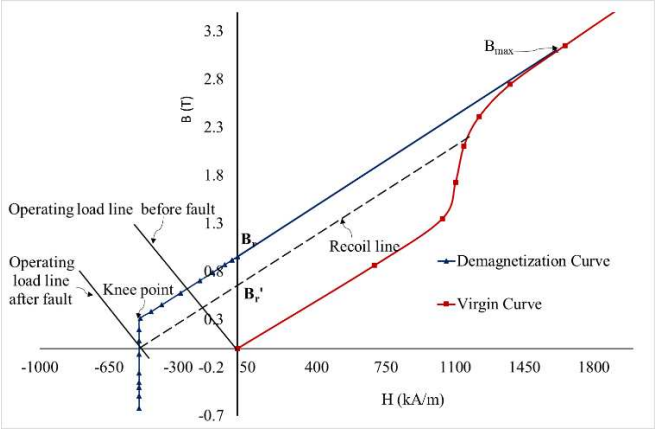

Fig. 1. Demagnetization B-H curve with virgin curve for the material L35EHT at 180º C explaining partial demagnetization.

The approach employed in this study uses B-H curve in the second and the third quadrant to consider demagnetization, while the virgin curve of the magnets shown in Fig.1 is used to determine the initial material magnetization in the absence of external fields [34]. Sintered Neodymium-Iron-Boron (NdFeB) magnets of grade N35EH with its B-H characteristics [35] shown in Fig.2 is used for study in this paper. To start with the analysis, flux density components, $B_{mag}X_{pn}$ and $B_{mag}Y_{pn}$, referred in the XY coordinate system shown in Fig. 3 for each magnet element are calculated individually based on their angle of magnetization θ_p as,

$$B_{mag}X_{pn} = B_{\max}\cos\theta_p, \quad B_{mag}Y_{pn} = B_{\max}\sin\theta_p. \tag{1}$$

where $B_{\max}$ is the saturation flux density achieved in magnet during its magnetization which is the flux density at the intersection of the B-H curve with the virgin curve as shown in

Fig.1, and the subscript 'n' denotes the n^{th} element of the p^{th} magnet. An example of the decomposition of $B_{\max}$ for the n^{th} magnet element in the p^{th} magnet (p=1 and 2) is shown in Fig.3. The magnetization of each magnet element is calculated in (1) and the slope is decided by the recoil permeability of the magnets. After the first step of the transient FE the flux density B_{pn} in the direction of magnetization observed in each element n of the p^{th} magnet is decomposed in to the X-Y components given by,

$$B_{demag}X_{pn} = B_{pn}\cos\theta_p.$$
$$B_{demag}Y_{pn} = B_{pn}\sin\theta_p. \quad (2)$$

The B-H curve model for each element is updated and stored based on the flux density values calculated by (2). This process repeats in every transient step, thus maintaining the information regarding the minimum flux density observed for every element of the magnets during its course of operation. If the flux density in a magnet element during a transient step is above the knee point of the material B-H curve for a given temperature, the remanence defined for the element will not be changed. If, however, the flux density is below the knee point, the B-H curve of the element for the subsequent step will be redefined by plotting a recoil line generated from the new minimum flux density as shown in the Fig.1.This calculation is repeated for every element, and hence different elements of a magnet might be operating on different magnetization levels following an event of uneven demagnetization. The new value of minimum flux density calculated in the X and Y directions is updated and stored for all those elements which have their flux density value gone below their previously updated value before proceeding for the following step. The whole process of demagnetization analysis is illustrated in the flow chart shown in the Fig.4.

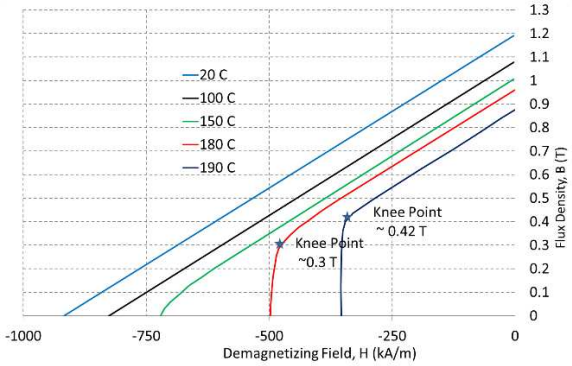

Fig.2. Demagnetization characteristics of N35EH magnet.

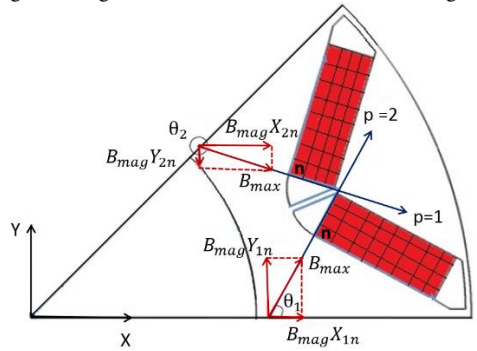

Fig.3. Decomposition of element flux density of a magnet in the direction of magnetization.

To evaluate the extent of partial demagnetization after operation, the magnitude of the minimum value of the flux density achieved in the n^{th} element of p^{th} magnet along the direction of magnetization can be calculated as

$$B(\min)_n = B_{demag}X_n\cos\theta_p + B_{demag}Y_n\sin\theta_p. \quad (3)$$

It is evident that partial demagnetization is said to have occurred if this value has gone below 0.3T at 180ºC and 0.42T at 190ºC, as shown in the Fig.2. These values can be identified as the knee point flux densities for the corresponding BH curves, as the curves change their slope from the product of relative permeability of the magnet material and the permeability of the free space ($\mu_r\mu_0$) to a much higher value at them. By assessing the minimum flux density in each element of every magnet, the percentage of the demagnetization of the magnet can be evaluated for a particular temperature of operation. This method can be extended to any operating temperature by providing corresponding temperature dependent B-H curves for the magnet under consideration.

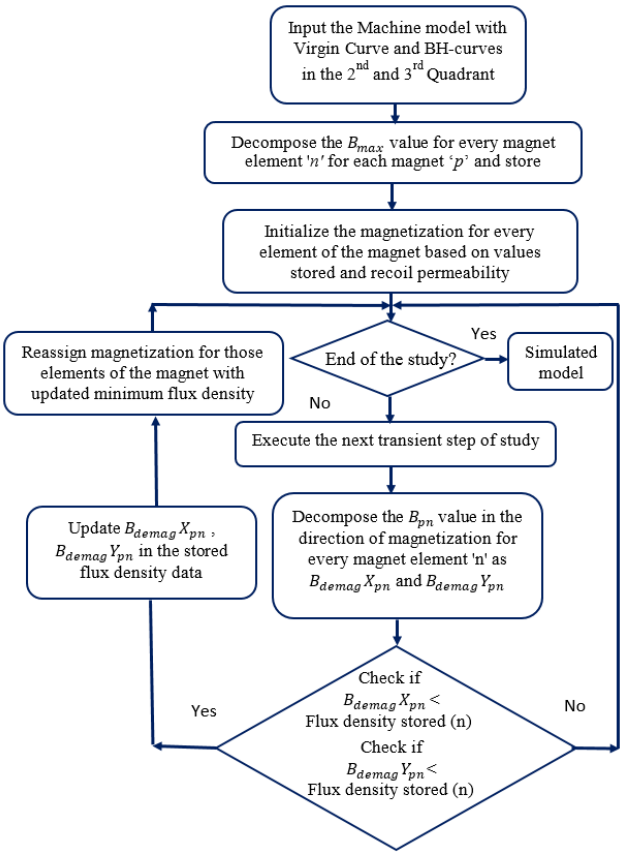

Fig.4. Flow chart of partial – demagnetization analysis of proposed model.

III. Case Studies

Without loss of generality, a 6-phase, 18 slot, 8-pole fractional slot IPM machine is considered in this study. The machine is developed to improve safety and to enhance drivetrain availability in traction application [15]. This machine has enhanced availability inherently [36], as loss of one 3-phase system will not lead to a complete loss of traction power. The cross-section of the PM machine is shown in the Fig.5. The machine winding consists of three series connected coils wired around the adjacent teeth with polarity as indicated by "+" and

"-", and phases denoted as A, B, C, D, E, and F. The magnets are shown in red and green as indicated by MiPj, where i = 1, 2 denotes ith magnet of the jth rotor pole (j = 1 to 8). The phase shift between A-B-C and D-E-F windings is 20º electrical, which is achieved by 13 slot-shifts [37]. The design parameters of the machine and the performance at the rated and the peak torque with magnet properties at 150ºC is tabulated in Table I and Table II respectively of [18] .

The 2-D transient FEA of the machine is carried out using the commercial FEA software in which the demagnetization model described in section II is implemented. M270-35A electrical steel is used for both the stator and the rotor laminations. For the demagnetization analyses, operating temperature of 180ºC is considered. For 2-D transient FEA, the current sources are connected in parallel with the switches which can be turned on at a specific rotor position with regard to the line-to-line voltage at its zero or peak when a short-circuit fault occurs. For considering the voltage reversal due to controller losing synchronization, voltage sources are connected in parallel to the current sources separated with switches which can be turned on in sequence without affecting each other.

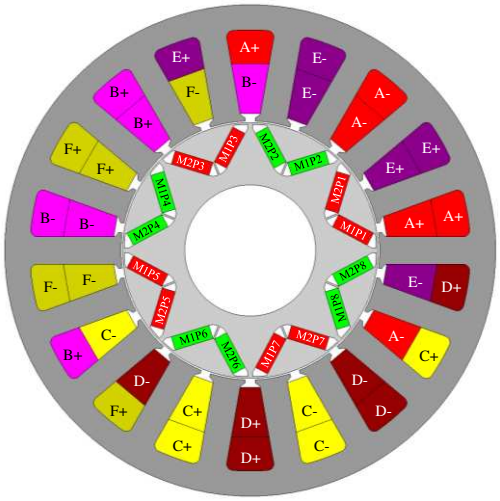

Fig. 5. Cross-section of 6-phase, 18-slot, 8-pole IPM machine

The study focuses on the fault conditions, listed in the Table I, which are most critical with respect to partial irreversible demagnetization. Faults F1 to F6 are short circuit faults while F7 to F12 considers the worse scenarios when the voltage vector has erroneous 180 electrical degree offset with respect to the back EMF due to faults in the position sensor and/or the controller.

A. Demagnetization Assessment for Short Circuit Faults

Table II gives the post demagnetization assessment in terms of reduction in back EMF and the reduction in the rated and the peak torque in percentage for the faults F1 to F6. Due to presence of sub-MMF harmonics in the fractional slot PM machine [15] and [18], partial demagnetization in each pole is slightly different. Hence, the reduction of the back EMF varies in a narrow range for the faults F1 to F4. It can be seen that the machine performance is not affected by short circuit faults F5 and F6 while it is most affected in F2. Fig.6 compares the increase in current to generate the rated and the peak torque after the short circuit faults F1 to F6. As the faults F5 and F6 have not caused any partial demagnetization the rated and the peak currents are not affected as indicated in the figure with a doted horizontal line.

Table III compares the maximum phase currents, peak demagnetizing currents (d axis currents) and the steady state short circuit current obtained by the proposed method with respect to the method described in [18] where continuous demagnetization is not accounted. Table IV compares the percentage of partial demagnetization in all the magnets calculated from the demagnetization tables during faults, F1 to F6. If flux density in a magnet element is below the knee point when a post-fault steady-state is reached, this element is considered to be partially demagnetized, although its remanence may still be close to that without demagnetization

TABLE I
FAULT CONDITIONS UNDER CONSIDERATION

	Fault	Pre-fault operation	Torque (N·m)	Speed (rpm)
F1	6-phase short-circuit	Rated torque	75	2800
F2	6-phase short-circuit	Peak torque	140	2800
F3	3-phase short-circuit	Rated torque	75	2800
F4	3-phase short-circuit	Peak torque	140	2800
F5	6-phase short circuit	Rated power	19.1	11000
F6	6-phase short circuit	Peak Power	27.8	11000
F7	6-phase voltage reversal	Rated torque	75	2800
F8	6-phase voltage reversal	Peak torque	140	2800
F9	3-phase voltage reversal	Rated torque	75	2800
F10	3-phase voltage reversal	Peak torque	140	2800
F11	6-phase voltage reversal	Rated power	19.1	11000
F12	6-phase voltage reversal	Peak power	27.8	11000

TABLE II

POST DEMAGNETIZATION ASSESSMENT FAULTS F1 TO F6

Fault	% Reduction in Back emf	% reduction in Torque	
		Rated	Peak
F1	1.85 to 1.96	0.91	1.49
F2	4.06 to 5.38	2.43	3.6
F3	0.42 to 0.58	0.21	0.42
F4	3.07 to 4.75	1.9	2.57
F5	0	0	0
F6	0	0	0

TABLE III
COMPARISON OF CURRENTS FOR OLD METHOD AND PROPOSED METHOD UNDER VARIOUS FAULT CONDITIONS

	F1		F2		F3		F4		F5		F6	
	Old Metd.	Prop. Metd.	Old Metd.	Prop. Metd.	Old Metd.	Prop. Metd.	Old Metd.	Prop. Metd.	Old Metd.	Prop. Metd.	Old Metd.	Prop. Metd.
Maximum phase current (A)	215.6	212	245.8	236	201.6	198	225.5	224	134.5	134.5	136.1	136.1
Maximum d-axis current (A)	-193.7	-184	-227.3	-235	-201.6	-200	-254.7	-236	-122.3	-122.3	-120.3	-120.3
Steady-state short circuit current (A)	-79.5	-74.85	-79.5	-72.3	-79.5	-75.2	-79.5	-73.3	-79.5	-79.5	-79.5	-79.5

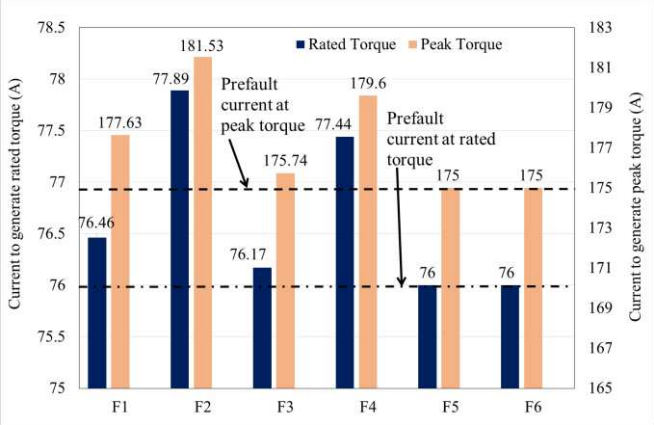

Fig. 6. Comparison of post fault current when magnet properties at 150ºC for generating rated and peak torque. (Faults F1 to F6)

TABLE IV
COMPARISON OF THE PERCENTAGE PARTIAL DEMAGNETIZED AREAS OBSERVED IN ALL MAGNETS UNDER VARIOUS FAULT CONDITIONS

	F1	F2	F3	F4	F5	F6
M_1P_1	10.2	15.3	8.4	17.1	0.1	0.2
M_1P_2	8.2	10.2	6.2	15.0	0.0	0.1
M_2P_1	68.1	85.6	12.2	27.3	0.0	0.0
M_2P_2	75.4	87.7	10.1	20.4	0.1	0.0
M_1P_3	45.2	67.4	12.3	25.2	0.1	0.0
M_2P_3	50.2	55.3	9.1	17.0	0.0	0.1
M_1P_4	6.0	7.2	7.3	12.1	0.2	0.1
M_2P_4	5.2	5.2	2.4	7.3	0.0	0.0
M_1P_5	72.4	93.2	20.6	72.4	0.0	0.0
M_2P_5	80.5	97.2	16.3	64.4	0.0	0.1
M_1P_6	8.4	16.2	12.2	22.1	0.0	0.0
M_2P_6	9.2	12.2	6.1	14.0	0.0	0.1
M_1P_7	5.4	7.3	4.3	13.2	0.0	0.0
M_2P_7	5.2	8.1	4.2	11.4	0.0	0.0
M_1P_8	68.3	82.2	11.1	23.1	0.1	0.2
M_2P_8	72.4	89.1	7.0	16.7	0.2	0.0

From these results following observations can be made about the post fault performance. The peak demagnetizing current has a significant impact on the partial demagnetization of the magnets. With an increase in pre-fault operating current, the peak demagnetizing current during fault transient also increases and, hence the magnets are more susceptible for partial demagnetization. In the case of 3- phase faults, the minimum average flux density observed is lower with respect to the 6-phase faults in some of the magnets, but the overall percentage demagnetization is comparatively lower. This makes the post fault performance after 3-phase faults slightly better than 6-phase faults with the same pre fault current. It is also seen that the steady state short circuit currents are reduced as a result of partial demagnetization compared to the method reported in [18] where post-fault performance analysis is not possible and the steady-state short circuit currents are computed by FE assuming the magnets are not demagnetized. The variation in percentage demagnetization among the magnets indicates the non-uniform demagnetization due to the presence of lower order MMF space harmonics in the fractional-slot PM machine. Fig.7 (a) and Fig.7 (b) shows the comparison of the demagnetized regions in the magnets for the worst affected faults F2 and F4, reinstating the uneven distributions of partially demagnetized areas. However, even though the percentage of the demagnetized areas under these conditions are quite high, the reduction in remanence seen in many partially demagnetized areas is relatively small, hence torque reduction is also relatively small. It is also worth noting that the reduction in the post fault torque capability is not proportional to the percentage of demagnetization. For example, partial demagnetized areas under faults F1 and F4 are 36.8% and 23.7% respectively. However, more reduction in torque under F4 is seen.

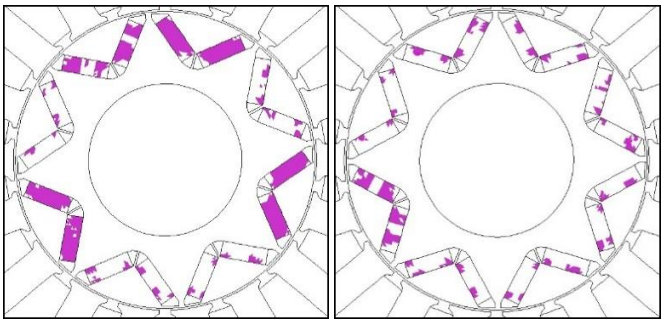

(a) 6-phase SC at T_{peak} (b) 3-phase SC at T_{peak}

Fig.7 Comparison of demagnetized regions after short circuit faults.

B. Demagnetization Assessment for Voltage Reversal.

A set of more severe faults with respect to demagnetization, F7 to F12, attributed to the voltage reversal resulting from inverter losing synchronization with respect to the back EMF voltages of the phases, due to sensing error or inverter fault are investigated here. Since the machine has two separate 3-phase winding systems, the failure due to one set of 3-phase supply losing synchronization and all the 6–phases losing synchronization are simulated separately to assess the partial demagnetization. Table V compares the peak phase current, the maximum d-axis current and the corresponding q-axis current during faults F7 to F12. Table VI shows the reduction in back EMF voltage and reduction in the rated and the peak torque as a result of demagnetization associated with faults F7 to F12. The results from the post demagnetization table indicate that all faults, F7 to F12, have resulted in far more significant partial demagnetization of the magnets. Fig. 8 indicates the increase in the rated current and the peak current in order to produce the rated and the peak torque after the partial demagnetization has occurred. Table VII compares the average value of the minimum flux density in the partially demagnetized regions of all the magnets during various faults, F7 to F12. The extent of partial demagnetization is not shown as a table because only small regions of the magnets from faults F11 and F12 has not under gone some degree of partial demagnetization, while every element of each magnets has gone below 0.3T in Faults F7 to F10.

The following observations can be made from the results obtained from the simulation of Faults F7 to F12. First the value of maximum d-axis current during the faults, not the peak phase current prior to the fault, influences the extent of partial demagnetization. Fault F9 has created the maximum demagnetizing current which pushes the minimum average flux

density in the magnet M2P3 to -1.91T. It is observed that the 3-phase voltage reversal faults (F10 & F12) could create the maximum demagnetization current comparable to the 6-phase voltage reversal faults (F7 & F8) for the same pre-fault currents even with the currents in the healthy 3-phase under faults F10 & F12 are not affected. This is because of the mutual magnetic coupling between the faulty phases and the heathy phases in the 3-phase reversal faults. Further the post-fault currents to generate the peak torque after faults F7 to F10 are closer to the maximum 6 – phase short circuit current for a healthy machine at 150^0C. Thus, if adequate post fault de-rating is not applied further demagnetization is likely to take place when magnet temperature is above 150^0C. It should also be noted from Table V that the fault currents associated with F11 and F12 at high speeds are much lower than those at the based speed. This is because in high speeds the machine exhibits high impedance which helps reduce the fault current and hence the severity of demagnetization. The extent of partial demagnetization not only depends on the maximum d –axis current, but also on time duration for which the magnets are exposed to it. This is because a longer duration makes more area of the magnet exposed to higher demagnetizing currents. For example, the maximum d-axis current in voltage reversal fault (F12) is marginally lower than that in short circuit fault (F2), but produces a more partially demagnetized areas. This is evident from the comparison of locus of the d- and q- axis currents for faults F2 and F12 as shown in the Fig.9. It is also worth noting from Fig.8 that the percentage increase of current in generating the torque at the rated conditions is lower than that at the peak load conditions. This can be accounted by the combined effect of reduction in the magnet torque due to lower remanence as a result of partial demagnetization and the reduction in the reluctance torque due to increased saturation.

TABLE V

COMPARISON OF PEAK CURRENTS(A): FAULTS F7 TO F12

Fault	Maximum phase current	Maximum *d*-axis current	Corresponding *q*-axis current
F7	1745	-1323	-691
F8	1612	-1372	-489
F9	1415	-1473	-487
F10	1272	-1380	-361
F11	251	-228	8
F12	245	-231	12

TABLE VI

POST DEMAGNETIZATION ASSESSMENT FAULTS F7 TO F12

Fault	% Reduction in Back EMF	% reduction in Torque	
		Rated	Peak
F7	34.53 to 37.18	18.48	21.14
F8	31.04 to 40.49	19.27	22.05
F9	20.87 to 38.23	15.43	17.28
F10	20.34 to 37.32	14.77	17.01
F11	4.01 to 5.12	2.11	3.21
F12	5.67 to 6.29	3.94	4.61

TABLE VII

COMPARISON OF THE AVERAGE MINIMUM FLUX DENSITY (T) IN THE PARTIALLY DEMAGNETIZED REGIONS OF ALL MAGNETS UNDER VARIOUS FAULT CONDITIONS

	F7	F8	F9	F10	F11	F12
M_1P_1	-0.52	-0.58	-0.55	-0.33	0.13	0.15
M_1P_2	-0.88	-0.62	-0.35	-0.42	0.10	0.11
M_2P_1	-0.53	-1.13	-0.63	-0.57	0.15	0.16
M_2P_2	-0.62	-0.61	-0.83	-0.61	0.16	0.16
M_1P_3	-0.91	-0.96	-0.53	-0.80	0.08	0.12
M_2P_3	-1.01	-0.98	-1.91	-0.76	0.09	0.11
M_1P_4	-0.49	-0.54	-0.82	-1.77	0.12	0.13
M_2P_4	-0.63	-0.52	-0.90	-0.79	0.14	0.15
M_1P_5	-1.17	-1.01	-0.99	-0.69	0.16	0.17
M_2P_5	-0.91	-1.00	-0.56	-0.79	0.15	0.17
M_1P_6	-0.67	-0.68	-0.38	-0.50	0.13	0.13
M_2P_6	-0.85	-0.93	-0.17	-0.09	0.10	0.09
M_1P_7	-0.73	-0.75	-0.29	-0.67	0.14	0.17
M_2P_7	-0.97	-0.96	-0.26	-0.51	0.12	0.17
M_1P_8	-1.31	-1.55	-0.65	-0.43	0.06	0.07
M_2P_8	-1.10	-1.09	-0.54	-0.41	0.08	0.09

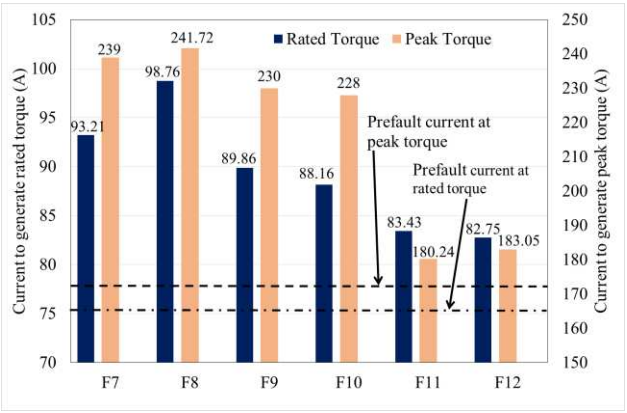

Fig. 8. Comparison of post fault current when magnet properties at 150ºC for generating rated and peak torque. (Faults F7 to F12)

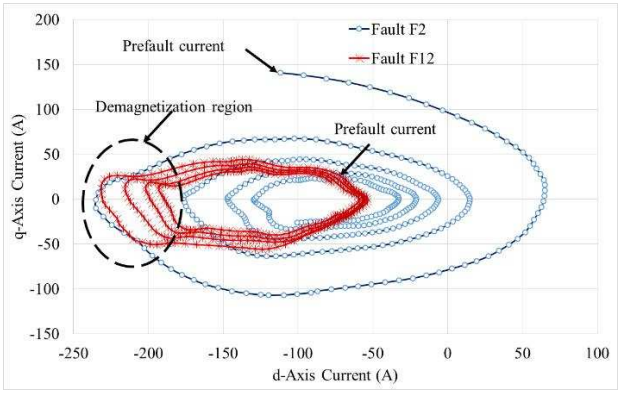

Fig.9. Comparison of locus of d and q axis current for the Faults F2 and F12.

IV. EXPERIMENTAL VALIDATION

A. *Experimental Testing Leading to Partial Demagnetization*

In order to validate the foregoing analysis of partial irreversible demagnetization, tests have been performed on the prototype IPM machine. The schematic of the inverter control system having independent control for both set of three phase system and also the experimental set up is explained in [36]. It

was operated at reduced dc link voltage (250V) compared to rated value (320V) and the testing was continued beyond its maximum operating speed (8600 r/min for 250V) with a torque demand of 20Nm so that the required current is deliberately increased under the deep flux weakening conditions. When dynamometer speed was increased from 10500 r/min to 10750 r/min, the motor was running under control for about 30s followed by one set of 3-phase system (A-B-C) losing synchronization with the voltage vector being opposite to the back-EMF, leading to much higher currents. The torque, armature currents, machine acceleration and speed captured against time during the experiment is shown in the Fig.10. However, due to limited storage capacity, the data was recorded only for every 20ms, and therefore the peak surge in ABC current magnitude was not captured. When the frictional torque of the machine is included, the electromagnetic torque before the fault transient is ~ 16 N·m.

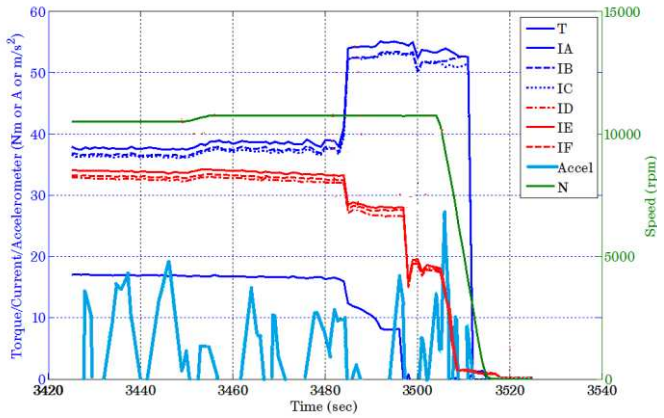

Fig. 10. Sequence of events during the incident of partial demagnetization of the prototype motor.

B. Electromagnetic and Thermal Analysis of the Test Condition.

Since the rotor temperature was not measured, electromagnetic and thermal analysis with the machine model calibrated by the measurement data at the rated and the peak conditions is used to estimate the rotor temperature. In deep field weakening operation, higher concentration of flux towards the rotor and higher order harmonics penetrating deeply inside the rotor increase the rotor losses in fractional-slot PM machines. Losses analysis is carried out in FEA at 10750 rpm with 16 N·m (measured torque at the time of experiment while losing synchronization) while operating at 250 V. The results from the loss evaluation and the thermal analysis are shown in Table VIII. It is seen that the rotor magnet temperature has gone up to 194.8ºC which is almost 30ºC higher than that would have been at 320 V DC link voltage. It is found that peak d- and q-axis currents of the faulted A-B-C system has reached 175A and 50A respectively during the time when the inverter losing synchronization.

C. Replicating the Experiment of Partial Demagnetization in FE Using Continuous Demagnetization Model.

It is clear from the above analysis that the magnet temperature was close to 190^{0}C and the peak transient currents in the ABC phases was close to 180A in the experiment. The same experiment sequence shown in the Fig.10 is repeated in FEA with continues demagnetization model enabled, supplied with demagnetization curve for the magnetic material at 190^{0}C. At a speed of 10750 r/min, phase D-E-F was carrying current close to 48A peak, while 52A peak current was flowing in phase A-B-C. A sudden voltage reversal is applied for 0.1ms allowing the transients to flow in A-B-C system. It is observed that the peak transient current is close to 185A in phase-A as obtained from the drive system simulations discussed previously. The rest of the experiment is repeated as in the Fig.10 but at reduced time scale as this part has not much to do with the partial demagnetization. Fig.11 shows the sequence at which phase currents are applied for the FE demagnetization model for repeating the experimental process.

TABLE VIII
RESULTS OF LOSS EVALUATION AND TEMPERATURE ESTIMATION

DC link voltage	**250 V**
Torque produced	15.8 (N.m)
Line-line voltage (fundamental)	237.8 V
Copper loss	597 W
Iron loss – stator	528 W
Iron loss – rotor	280 W
Eddy current loss in magnets	57 W
Total rotor loss to be dissipated	337 W
Rotor back iron temperature	195.4ºC
Rotor magnet temperature	194.8ºC
Rotor surface temperature	191.8ºC
Stator surface temperature	113.4ºC
Average winding temperature	116.5ºC

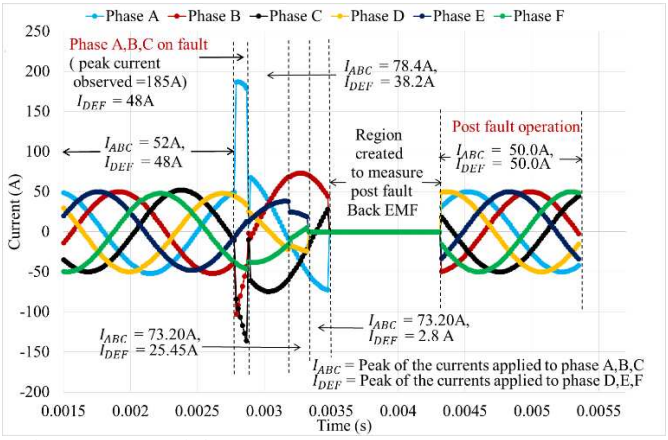

Fig.11 Sequence of phase current's applied /observed in demagnetization model to replicate the experiment.

D. Post Demagnetization Performance Following the Loss of Synchronization.

Post the demagnetization, the back-EMF measurements were taken to quantify the effect of demagnetization. It is observed that the back EMF of the motor is reduced by ~26% compared to the measured value during healthy operation, confirming partial demagnetization of the rotor magnets. The comparison of the actual back EMF measured at 2800 r/min after the

demagnetization experiment and the FE simulation predictions from the continuous demagnetization model is shown in the Fig.12. The result indicates that the peak of the measured back EMF has a variation of 19.25 to 28.52% while the simulations showing a variation of 15.1 to 27.0%. The comparison of the average value of the measured torque before and after the partial demagnetization with the simulated value after partial demagnetization at rated dc link voltage is shown in the Fig.13. It is observed at 11000 r/min that the measured torque is reduced to 16.2 Nm from 19 Nm while the simulation shows it is reduced to an average value of 16.5 Nm. This validates the FE model for continuous demagnetization presented in this paper. It should be noted that the percentage of torque reduction is lower than that of the back EMF, since the torque produced by the PM field contributes to ~60% of the total torque. The rest is the reluctance torque which is not affected by the partial demagnetization. Hence the machine can be operated further with a reduced rated toque capacity by about 17% which corresponds to 28% reduction in the magnet torque because of partial demagnetization. The derating of the machine is necessary in order to prevent overheating and hence potentially further demagnetization.

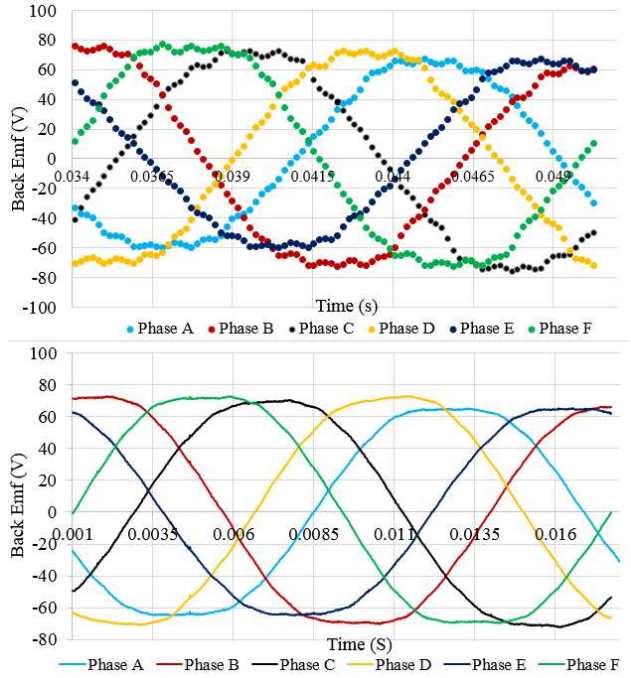

Fig.12 Comparison of post fault back EMF from the continuous demagnetization model (top plot) and the experimental value (bottom plot).

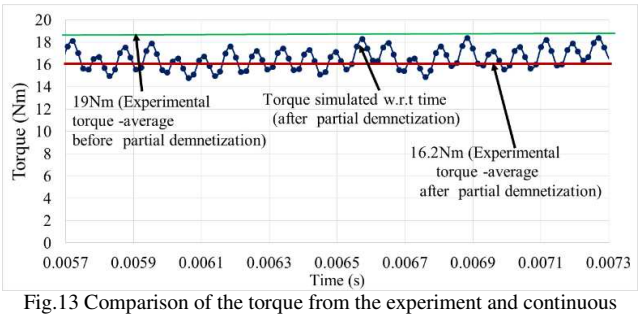

Fig.13 Comparison of the torque from the experiment and continuous demagnetization model (dc link voltage: 320V).

V. Conclusion

The partial demagnetization of an IPM machine with fractional-slot per pole winding configuration has been comprehensively assessed under worst operating conditions using the described method. It has been shown that although partially demagnetized areas are quite large under the worst short-circuit conditions, the reduction of machine torque capability is relatively small. Voltage reversal caused by position sensor failure or controller failure leads to a far severe demagnetization on the machine and the resultant demagnetization current could be an order of magnitude greater than the rated current. The demagnetized model is employed for predicting post fault machine performance and the phase currents required for given torque at any load conditions following a fault condition that has led to partial demagnetization. This helps in making more reliable and robust machine against all potential fault scenarios, during the design phase, and also to quantify derating of the machine for subsequent usage to prevent any further partial demagnetization while in operation. The assessment technique has been validated by demagnetization experiments on a prototype machine, and is applicable to any PM machines.

References

[1] L. Parsa and H. A. Toliyat, "Fault-Tolerant Interior-Permanent-Magnet Machines for Hybrid Electric Vehicle Applications," *Vehicular Technology, IEEE Transactions on,* vol. 56, pp. 1546-1552, 2007.

[2] M. Barcaro, A. Faggion, L. Sgarbossa, N. Bianchi, and S. Bolognani, "Performance evaluation of an integrated starter alternator using an interior permanent magnet machine," *Electric Power Applications, IET,* vol. 4, pp. 539-546, 2010.

[3] A. Wang, Y. Jia, and W. L. Soong, "Comparison of Five Topologies for an Interior Permanent-Magnet Machine for a Hybrid Electric Vehicle," *Magnetics, IEEE Transactions on,* vol. 47, pp. 3606-3609, 2011.

[4] L. Sun-Kwon, K. Gyu-Hong, and H. Jin, "Finite Element Computation of Magnetic Vibration Sources in 100 kW Two Fractional-Slot Interior Permanent Magnet Machines for Ship," *Magnetics, IEEE Transactions on,* vol. 48, pp. 867-870, 2012.

[5] T. M. Jahns and R. C. Van Nocker, "High-performance EHA controls using an interior permanent magnet motor," *Aerospace and Electronic Systems, IEEE Transactions on,* vol. 26, pp. 534-542, 1990.

[6] F. Parasiliti, M. Villani, S. Lucidi, and F. Rinaldi, "Finite-Element-Based Multiobjective Design Optimization Procedure of Interior Permanent Magnet Synchronous Motors for Wide Constant-Power Region Operation," *Industrial Electronics, IEEE Transactions on,* vol. 59, pp. 2503-2514, 2012.

[7] T. M. Jahns, "Flux-Weakening Regime Operation of an Interior Permanent-Magnet Synchronous Motor Drive," *Industry Applications, IEEE Transactions on,* vol. IA-23, pp. 681-689, 1987.

[8] A. Sarikhani and O. A. Mohammed, "Demagnetization Control for Reliable Flux Weakening Control in PM Synchronous Machine," *Energy Conversion, IEEE Transactions on,* vol. 27, pp. 1046-1055, 2012.

[9] K. Atallah, W. Jiabin, and D. Howe, "Torque-ripple minimization in modular permanent-magnet brushless machines," *Industry Applications, IEEE Transactions on,* vol. 39, pp. 1689-1695, 2003.

[10] W. Jiabin, X. Ping, Z., and D. Howe, "Three-phase modular permanent magnet brushless Machine for torque boosting on a downsized ICE vehicle," *Vehicular Technology, IEEE Transactions on,* vol. 54, pp. 809-816, 2005.

[11] A. M. El-Refaie, J. P. Alexander, S. Galioto, P. B. Reddy, H. Kum-Kang, P. de Bock, *et al.*, "Advanced High-Power-Density Interior Permanent Magnet Motor for Traction Applications," *Industry Applications, IEEE Transactions on,* vol. 50, pp. 3235-3248, 2014.

[12] D. Ishak, Z. Q. Zhu, and D. Howe, "Eddy-current loss in the rotor magnets of permanent-magnet brushless machines having a fractional number of slots per pole," *Magnetics, IEEE Transactions on,* vol. 41, pp. 2462-2469, 2005.

[13] J. Wang, K. Atallah, R. Chin, W. M. Arshad, and H. Lendenmann, "Rotor Eddy-Current Loss in Permanent-Magnet Brushless AC Machines," *Magnetics, IEEE Transactions on,* vol. 46, pp. 2701-2707, 2010.
[14] K. Yamazaki, Y. Kanou, Y. Fukushima, S. Ohki, A. Nezu, T. Ikemi*, et al.*, "Reduction of Magnet Eddy-Current Loss in Interior Permanent-Magnet Motors With Concentrated Windings," *Industry Applications, IEEE Transactions on,* vol. 46, pp. 2434-2441, 2010.
[15] V. I. Patel, J. Wang, W. Wang, and X. Chen, "Six-Phase Fractional-Slot-per-Pole-per-Phase Permanent-Magnet Machines With Low Space Harmonics for Electric Vehicle Application," *Industry Applications, IEEE Transactions on,* vol. 50, pp. 2554-2563, 2014.
[16] A. Vagati, B. Boazzo, P. Guglielmi, and G. Pellegrino, "Design of Ferrite-Assisted Synchronous Reluctance Machines Robust Toward Demagnetization," *Industry Applications, IEEE Transactions on,* vol. 50, pp. 1768-1779, 2014.
[17] V. I. Patel and J. Wang, "Demagnetization assessment of 6-phase fractional-slot permanent magnet machines with low space harmonics under various fault conditions," in *Power Electronics, Machines and Drives (PEMD 2014), 7th IET International Conference on*, 2014, pp. 1-6.
[18] V. I. Patel, J. Wang, and S. S. Nair, "Demagnetization Assessment of Fractional-Slot and Distributed Wound 6-Phase Permanent Magnet Machines," *Magnetics, IEEE Transactions on,* vol. 51, pp. 1-11, 2015.
[19] B. M. Ebrahimi and J. Faiz, "Demagnetization Fault Diagnosis in Surface Mounted Permanent Magnet Synchronous Motors," *Magnetics, IEEE Transactions on,* vol. 49, pp. 1185-1192, 2013.
[20] H. Jongman, P. Sanguk, H. Doosoo, K. Tae-june, L. Sang Bin, C. Kral*, et al.*, "Detection and Classification of Rotor Demagnetization and Eccentricity Faults for PM Synchronous Motors," *Industry Applications, IEEE Transactions on,* vol. 48, pp. 923-932, 2012.
[21] W. Jiabin, W. Wang, K. Atallah, and D. Howe, "Demagnetization Assessment for Three-Phase Tubular Brushless Permanent-Magnet Machines," *Magnetics, IEEE Transactions on,* vol. 44, pp. 2195-2203, 2008.
[22] K. Ki-Chan, K. Kwangsoo, K. Hee-jun, and L. Ju, "Demagnetization Analysis of Permanent Magnets According to Rotor Types of Interior Permanent Magnet Synchronous Motor," *Magnetics, IEEE Transactions on,* vol. 45, pp. 2799-2802, 2009.
[23] S. Ruoho, E. Dlala, and A. Arkkio, "Comparison of Demagnetization Models for Finite-Element Analysis of Permanent-Magnet Synchronous Machines," *Magnetics, IEEE Transactions on,* vol. 43, pp. 3964-3968, 2007.
[24] K. Gyu-Hong, H. Jin, N. Hyuk, H. Jung-Pyo, and K. Gyu-Tak, "Analysis of irreversible magnet demagnetization in line-start motors based on the finite-element method," *Magnetics, IEEE Transactions on,* vol. 39, pp. 1488-1491, 2003.
[25] Y. Zhilichev, "Analysis of Permanent Magnet Demagnetization Accounting for Minor B-H Curves," *Magnetics, IEEE Transactions on,* vol. 44, pp. 4285-4288, 2008.
[26] P. Zhou, D. Lin, Y. Xiao, N. Lambert, and M. A. Rahman, "Temperature-Dependent Demagnetization Model of Permanent Magnets for Finite Element Analysis," *Magnetics, IEEE Transactions on,* vol. 48, pp. 1031-1034, 2012.
[27] S. Ruoho, J. Kolehmainen, J. Ikaheimo, and A. Arkkio, "Interdependence of Demagnetization, Loading, and Temperature Rise in a Permanent-Magnet Synchronous Motor," *Magnetics, IEEE Transactions on,* vol. 46, pp. 949-953, 2010.
[28] K. Hyung-Kyu, H. Jin, K. Byeong-Woo, and K. Gyu-Hong, "Characteristic analysis of IPM type BLDC motor considering the demagnetization of PM by stator turn fault," in *Energy Conversion Congress and Exposition (ECCE), 2010 IEEE*, 2010, pp. 3063-3070.
[29] L. Yoon-Seok, K. Kyung-Tae, and H. Jin, "Finite-Element Analysis of the Demagnetization of IPM-Type BLDC Motor With Stator Turn Fault," *Magnetics, IEEE Transactions on,* vol. 50, pp. 889-892, 2014.
[30] K. Ki-Chan, L. Seung-Bin, K. Dae-Hyun, and L. Ju, "The Shape Design of Permanent Magnet for Permanent Magnet Synchronous Motor Considering Partial Demagnetization," *Magnetics, IEEE Transactions on,* vol. 42, pp. 3485-3487, 2006.
[31] C. Gilsu and T. M. Jahns, "Interior permanent magnet synchronous machine rotor demagnetization characteristics under fault conditions," in *Energy Conversion Congress and Exposition (ECCE), 2013 IEEE*, 2013, pp. 2500-2507.
[32] J. D. McFarland and T. M. Jahns, "Investigation of the Rotor Demagnetization Characteristics of Interior PM Synchronous Machines During Fault Conditions," *Industry Applications, IEEE Transactions on,* vol. 50, pp. 2768-2775, 2014.
[33] P. Campbell, *Permanent Magnet Materials and Their Applications. Cambridge, U. K.: Cambridge University Press,* pp. 90–97, 1994.
[34] U. G. OPERA-2D, Vector Fields Ltd., Oxford, U.K, 2013.
[35] A. M. Technologies, *Neodymium-Iron-Boron Magnet Catalogs. Available:* http://www.arnoldmagnetics.com/Neodymium_Literature.aspx.
[36] V. Patel, J. Wang, D. Nugraha, R. Vuletic, and J. Tousen, "Enhanced Availability of Drivetrain through Novel Multi-phase Permanent Magnet Machine Drive," *Industrial Electronics, IEEE Transactions on,* vol. PP, pp. 1-1, 2015.
[37] V. I. Patel, J. Wang, W. Wang, and C. Xiao, "Analysis and design of 6-phase fractional slot per pole per phase permanent magnet machines with low space harmonics," in *Electric Machines & Drives Conference (IEMDC), 2013 IEEE International*, 2013, pp. 386-393.

Sreeju S. Nair (S'14) received the B.Tech. in electrical engineering from National Institute of Technology, Calicut, India in 2002. and M.Tech. in power systems and power electronics from Indian Institute of Technology, Madras, India in 2006.

From 2002 to 2004, he was a research fellow at Defence Research and Development Organization (DRDO), Hyderabad, India. In 2006, he worked as a development engineer for light commercial vehicles with Tata Motors, Pune, India. From 2007 to 2013, he was a Lead Engineer with TVS Motor Company Ltd. At present, he is pursuing the Ph.D. degree in electronic & electrical engineering at The University of Sheffield, Sheffield, U.K. His research interests include design and development of engine mounted and wheel mounted permanent-magnet machines for electric and hybrid vehicle applications.

Mr. Nair is a member of SAE since 2013.

Vipulkumar I. Patel (M'13) received the B.E. degree in electrical engineering from Nirma Institute of Technology, Gujarat University, Ahmedabad, India, in 2003, the M.Tech. degree in power electronics, electrical machines, and drives from the Indian Institute of Technology Delhi, New Delhi, India, in 2005, and Ph.D. degree in electronic and electrical engineering from The University of Sheffield, Sheffield, U.K., in 2014.

He is currently a Research Assistant in electronic and electrical engineering with The University of Sheffield. From 2005 to 2010, he was a Lead Engineer with the GE India Technology Centre, Bangalore, India. His research interests include design and analysis of permanent-magnet machines for electric traction applications.

Dr. Patel was a recipient of the IEEE Power Electronics, Drives and Energy Systems '96 Award for the Best Performance in the Area of Power Electronics, Electrical Machines & Drives in 2005.

Jiabin Wang (SM'03) received the B.Eng. and M.Eng. degrees from Jiangsu University of Science and Technology, Zhengjiang, China, in 1982 and 1986, respectively, and the Ph.D. degree from the University of East London, London, U.K., in 1996, all in electrical and electronic engineering.

Currently, he is a Professor in Electrical Engineering at the University of Sheffield, Sheffield, U.K. From 1986 to 1991, he was with the Department of Electrical Engineering at Jiangsu University of Science and Technology, where he was appointed a Lecturer in 1987 and an Associated Professor in 1990. He was a Postdoctoral Research Associate at the University of Sheffield, Sheffield, U.K., from 1996 to 1997, and a Senior Lecturer at the University of East London from 1998 to 2001. His research interests range from motion control and electromechanical energy conversion to electric drives for applications in automotive, renewable energy, household appliances and aerospace sectors.

He is a fellow of the IET and a senior member of IEEE.